PROCEEDINGS OF SCIENCE

Non-resonant and electroweak corrections to top pair production near threshold

Andreas Maier*
Institute for Particle Physics Phenomenology, Durham University, Durham, United Kingdom
E-mail: andreas.maier@durham.ac.uk

At lepton colliders, the top-quark mass can be extracted with unparalleled precision from the total production cross section of top-antitop decay products near threshold. We discuss next-to-next-to-leading order non-resonant and electroweak corrections to this observable and their impact on the determination of top-quark properties.

Loops and Legs in Quantum Field Theory (LL2018)
29 April 2018 - 04 May 2018
St. Goar, Germany

*Speaker.

PoS(LL2018)004

1. Introduction

Future high-energy electron-positron colliders will allow a clean determination of the top-quark mass in a well-defined mass scheme with unprecedented precision. The most sensitive observable in this respect is the total cross section for the process $e^+e^- \to b\bar{b}W^+W^-X$ near the top-pair production threshold. Preliminary studies [1, 2, 3, 4] suggest that the mass in the $\overline{\text{MS}}$ scheme can be determined with a precision of 50 MeV or better. In addition to the top-quark mass m_t, its width Γ_t and Yukawa coupling y_t as well as the strong coupling constant α_s can be extracted from the same measurement. Since the current theory uncertainties exceed the projected experimental error by far, it is essential to improve the theoretical prediction further.

The production of the final state $b\bar{b}W^+W^-X$ near the top-pair threshold is dominated by the creation and subsequent decay of a non-relativistic top-pair. Its lifetime is comparable to the typical time scale of bound-state formation via a colour Coulomb potential interaction. These effects can be treated systematically by combining potential non-relativistic effective field theory (PNREFT) [5, 6, 7] with unstable particle effective theory [8, 9]. We adopt the power counting $v \sim \alpha_s \sim \sqrt{\alpha} \sim y_t \ll 1$, where v is the heavy-quark velocity and α the electromagnetic coupling constant. The leading potential interaction scales with powers of $\alpha_s/v \sim 1$ and has to be resummed to all orders in perturbation theory. The same holds for the leading effects due to the top-quark decay width $\Gamma_t \sim \alpha m_t^2$, which scale with powers of $\alpha/v^2 \sim 1$.

Pure QCD corrections to the production cross section, involving only powers of the velocity and the strong coupling constant, were calculated up to next-to-next-to-next-to-leading order (NNNLO) in [10]. The final prediction exhibits good apparent convergence and a residual scale uncertainty of about 3%. A similar behaviour was found at NNLO with next-to-next-to-leading logarithmic resummation [11]. In the following we discuss higher-order corrections associated with the remaining Standard Model couplings, summarising the results of [12, 13]. These corrections cancel finite-width divergences in the QCD corrections and are therefore essential for obtaining a consistent prediction. Furthermore, depending on the centre-of-mass energy, the numeric effects can be sizeable and exceed the QCD uncertainty estimate significantly. Finally, corrections beyond QCD have to be included to assess the sensitivity of the cross section to variations in the top-quark Yukawa coupling.

2. Non-resonant and electroweak corrections

Various types of contributions arise from the electroweak and Higgs sector of the Standard Model. Corrections to production via a resonance manifest themselves in the creation and the propagation of the intermediate $t\bar{t}$ pair. A further important contribution is given by QED corrections to the initial state. Finally, the same final state $b\bar{b}W^+W^-X$ can be produced without creating a $t\bar{t}$ resonance.

2.1 Electroweak corrections to $t\bar{t}$ production

Electroweak corrections to the production of a $t\bar{t}$ resonance were calculated in [14, 15, 16, 17] at NNLO according to our power counting. Corrections involving only the strong coupling and the top-quark Yukawa coupling are even known at NNNLO [18].

The interaction potential between the top and the antitop receives a correction due to the QED Coulomb potential at NLO. While there are no further corrections at NNLO, we also include Higgs-boson exchange in the form of a local NNNLO potential [12]. Finally, based on the canonical parametrisation $p_t^2 = m_t^2 - im_t\Gamma_t$ for the complex top-quark pole, we obtain a NNLO correction of the form

$$\delta\mathscr{L}_{\psi,\mathrm{kin}} = \psi^\dagger \frac{\left(\vec{\partial}^2 + im_t\Gamma_t\right)^2}{8m_t^3}\psi \tag{2.1}$$

to the kinetic terms in the Lagrangian, where ψ is the non-relativistic top-quark field. There is an analogous correction for the antitop. The mixed term proportional to $\vec{\partial}^2\Gamma_t$ in Eq. (2.1) corresponds to a time dilatation correction due to the residual movement of the top quark. Consequently, it induces a small reduction in the width of the $t\bar{t}$ resonance [13].

2.2 Initial state radiation

The incoming e^+e^- state receives corrections from virtual photon exchange and the real radiation of photons with characteristic energies and momenta of the order of $m_t v^2$. In addition to a non-logarithmic contribution starting at NNLO [13], these corrections induce large logarithms $\alpha\log\frac{m_e}{m_t}$, where m_e is the small electron mass. Such logarithms can be resummed to all orders by performing a convolution with the electron structure function $\Gamma_{ee}^{\mathrm{LL}}$, which is known at leading-logarithmic accuracy [19, 20]. The resummed cross section σ_{ISR} is then given in terms of the "partonic" cross section σ^{conv} by

$$\sigma_{\mathrm{ISR}}(s) = \int_0^1 dx_1 \int_0^1 dx_2 \Gamma_{ee}^{\mathrm{LL}}(x_1)\Gamma_{ee}^{\mathrm{LL}}(x_2)\sigma^{\mathrm{conv}}(x_1x_2s)\,. \tag{2.2}$$

2.3 Non-resonant production

For a theoretically consistent treatment we also have to take into account the possibility of producing the final-state $t\bar{t}$ decay products without going through an intermediate $t\bar{t}$ resonance. According to unstable particle effective theory [8, 9], the overall cross section is given by the sum of the resonant production cross section discussed in the previous sections and the non-resonant cross section. While non-resonant production is suppressed with respect to resonant production by one power of α, its phase space is larger by a factor of the order of $1/v$. It therefore first contributes at NLO [21].

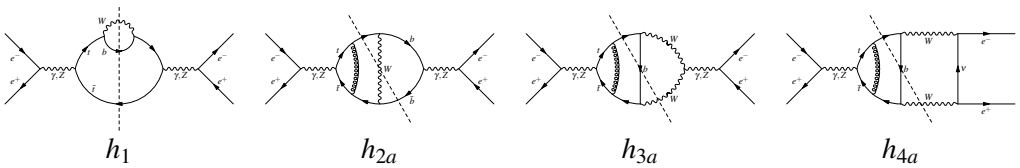

Figure 1: Sample diagrams contributing to the non-resonant cross section at NLO (h_1) and NNLO (h_{2a}, h_{3a}, h_{4a}).

Partial NNLO corrections were calculated in [22, 23]. The complete result was obtained recently in [13]. At this order, we have to consider the final states $t\bar{b}W^-$, $t\bar{b}W^-g$, $bW^+\bar{t}$, and $bW^+\bar{t}g$. Due to CP symmetry, it is sufficient to only consider the final states $bW^+\bar{t}$, $bW^+\bar{t}g$ and multiply

the resulting cross section by a factor of two. Sample NLO and NNLO diagrams are shown in Fig. 1. Unlike in the resonant contribution, virtual top quarks with momenta p_t are parametrically far off shell, $p_t^2 - m_t^2 \sim m_t^2 \gg m_t\Gamma_t$, and the width is not resummed into the propagators. This leads to endpoint divergences in phase-space regions were the virtual top quarks go on shell. These endpoint divergences cancel against the finite-width divergences in the resonant production cross section. Since the resonant contribution is calculated in dimensional regularisation, the endpoint divergences have to be regularised in the same way for consistency. A fully automated calculation of the NNLO non-resonant contribution using standard tools is therefore not possible.

Our strategy is to isolate and manually compute the endpoint-divergent parts and use standard automated methods for the endpoint-finite remainder. The total cross section can be decomposed as

$$\sigma = \sigma_{\text{res}} + \sigma_{\text{sq}} + \sigma_{\text{int}} + \sigma_{\text{aut}}\,, \tag{2.3}$$

where σ_{res} is the resonant contribution and the remaining terms constitute the non-resonant cross section. The "squared" cross section σ_{sq} is given by the sum of all virtual, real, and counterterm corrections to the diagram h_1 in Fig. 1. It is endpoint singular, but has no overall ultraviolet (UV) divergence. The remaining endpoint-divergent diagrams, h_{2a}, h_{3a}, h_{4a} in Fig. 1 and symmetric diagrams, are also UV divergent and together form the "interference" contribution σ_{int}. The "automated" cross section σ_{aut} in Eq. (2.3) comprises about 100 endpoint-finite diagrams, which are calculated with modified `Madgraph5_aMC@NLO` [24] code.

In order to consistently combine the resonant cross section σ_{res}, where the phase-space integration is performed in $d = 4 - 2\varepsilon$ dimensions, with the four-dimensional phase space integration performed in the "automated" part σ_{aut}, we have to identify separately finite pieces in Eq. (2.3) and compute each of these in a uniform scheme. To this end, we first split the "interference" contribution into an endpoint-divergent and ultraviolet-finite part and an endpoint-finite remainder:

$$\sigma_{\text{int}} = \sigma_{\text{int}}^{(\text{EP div})} + \sigma_{\text{int}}^{(\text{EP fin})}\,. \tag{2.4}$$

This can be achieved by considering the expansion of the phase-space integral over the rescaled top-quark invariant mass $t = \frac{p_t^2}{m_t^2}$ around the endpoint $t = 1$:

$$\int_y^1 dt\, g_{ix}(t) = \sum_{a=1,\frac{3}{2},2} \sum_n \frac{\hat{g}_{ix}^{(a,n)}(1-y)^{1-a-n\varepsilon}}{1-a-n\varepsilon} + \int_y^1 dt \left[g_{ix}(t) - \sum_{a=1,\frac{3}{2},2} \sum_n \frac{\hat{g}_{ix}^{(a,n)}}{(1-t)^{a+n\varepsilon}} \right]. \tag{2.5}$$

$y \geq 0$ parametrises a cut on the top-quark invariant mass. The first term on the right-hand-side of Eq. (2.3) originates from the expansion around the endpoint, where $\hat{g}_{ix}^{(a,n)}$ are expansion coefficients of the integrand g_{ix}. Consequently, the second term is endpoint finite. The combinations $\sigma_{\text{res}} + \sigma_{\text{sq}} + \sigma_{\text{int}}^{(\text{EP div})}$ and $\sigma_{\text{int}}^{(\text{EP fin})} + \sigma_{\text{aut}}$ are then separately finite and can be calculated in different schemes.

3. Impact on phenomenology

In Fig. 2 we demonstrate the impact of all beyond-QCD corrections except initial-state-radiation on $\sigma(e^+e^- \to b\bar{b}W^+W^-X)$. As parameters, we have chosen the top-quark mass in the potential-

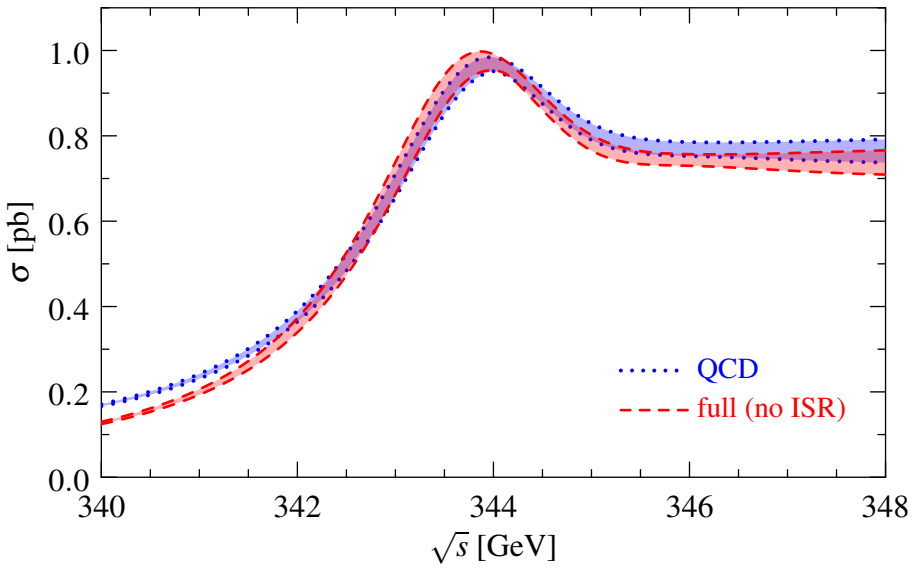

Figure 2: Comparison between the QCD (dotted blue) and full (dashed red) predictions for the total $b\bar{b}W^+W^-X$ production cross section. ISR corrections are not included.

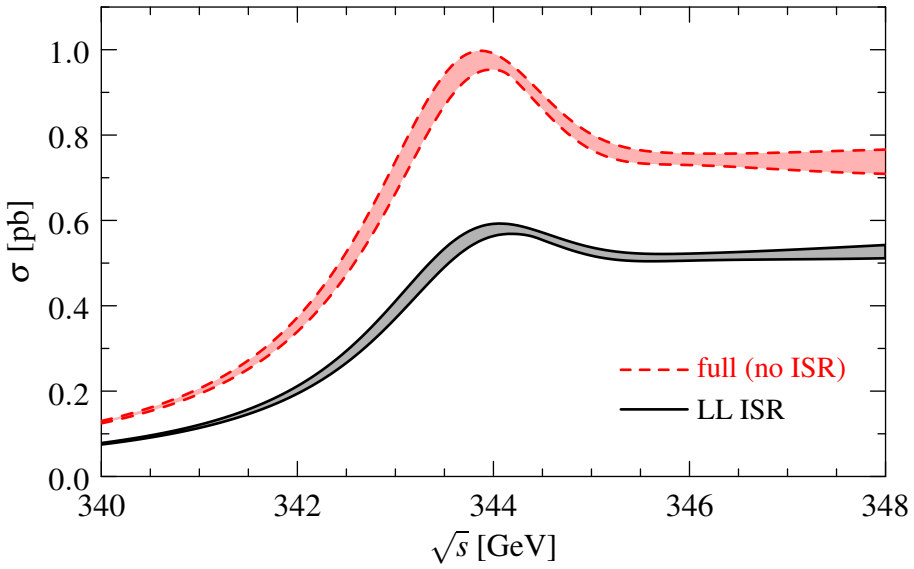

Figure 3: Comparison between the full cross section without (dashed red) and with (solid black) initial-state radiation.

subtracted scheme [25] $m_t^{\mathrm{PS}}(20\,\mathrm{GeV}) = 171.5\,\mathrm{GeV}$, the on-shell width $\Gamma_t = 1.33\,\mathrm{GeV}$, the Higgs-boson mass $m_H = 125\,\mathrm{GeV}$, the strong coupling $\alpha_s(m_Z) = 0.1184$ and the electromagnetic coupling $\alpha(m_Z) = 1/128.944$ at the Z pole with the weak-boson masses $m_W = 80.385\,\mathrm{GeV}, m_Z = 91.1876\,\mathrm{GeV}$. The uncertainty bands are obtained by varying the renormalisation scale between $\mu = 50\,\mathrm{GeV}$ and $\mu = 350\,\mathrm{GeV}$. In the peak region there is a significant cancellation between the various types of corrections and the overall change amounts to a minor enhancement with a slightly reduced peak width. For higher energies the corrections are significant and comparable to the scale

uncertainty. The largest relative change is observed below the peak, where the cross section is reduced by up to 25%. In Fig. 3, we show the effect of initial-state radiation. The peak is smeared out and the cross section is reduced drastically, by 30–45%.

The main purpose of a threshold scan is the determination of top-quark properties. In Fig. 4 we illustrate the sensitivity of the cross section to changes in the top-quark mass, width, Yukawa coupling, and the strong coupling. The changes in the cross section suggest sufficient sensitivity to measure mass shifts of about 50 MeV, which is in line with preliminary experimental studies [1, 2, 3, 4].

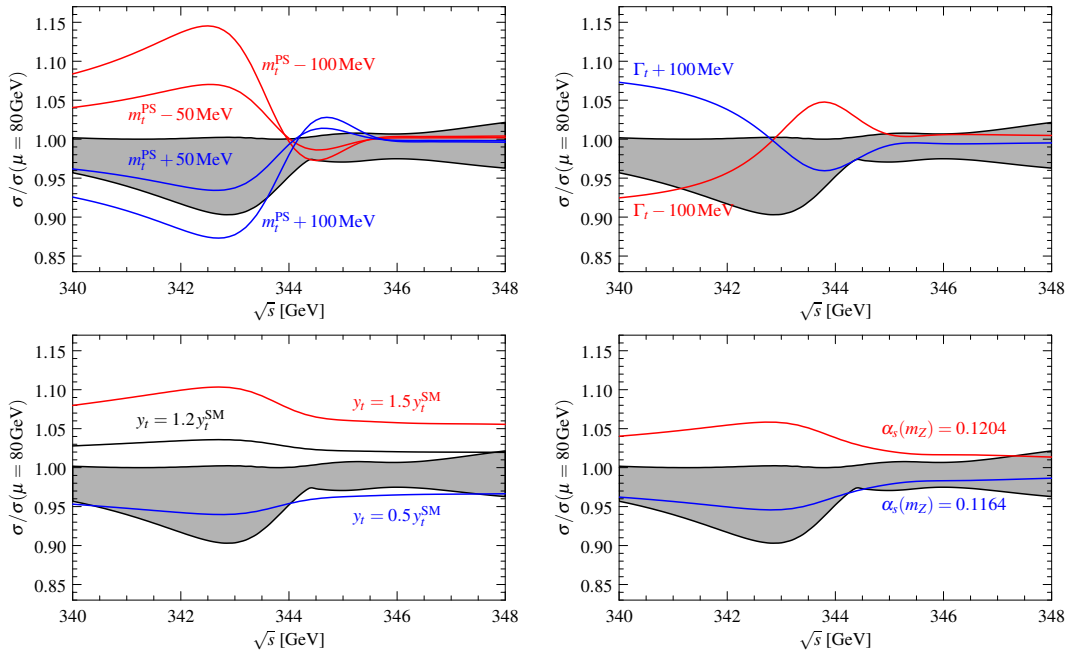

Figure 4: Sensitivity of the cross section to changes in the top-quark mass (top left panel), width (top right), Yukawa coupling (bottom left), and in the strong coupling (bottom right). The black band is the cross section with default parameters and scale variation between $\mu = 50\,\text{GeV}$ and $\mu = 350\,\text{GeV}$. All lines are normalised to the cross section at $\mu = 80\,\text{GeV}$.

4. Conclusions

NNLO electroweak and non-resonant corrections to the cross section for $e^+e^- \to b\bar{b}W^+W^-X$ near the top-antitop production threshold are both required for theoretical consistency and numerically sizeable in significant parts of the relevant energy range. A state-of-the-art theory prediction including NNNLO QCD and Higgs corrections and NNLO electroweak and non-resonant corrections supports the expectation of measuring the top-quark mass in a well-defined scheme with an uncertainty of about 50 MeV at a future lepton collider.

All corrections are included in version 2 of the public code `QQbar_threshold` [26, 13], available from `http://qqbarthreshold.hepforge.org/`.

References

[1] K. Seidel, F. Simon, M. Tesar and S. Poss, *Top quark mass measurements at and above threshold at CLIC*, *Eur. Phys. J.* **C73** (2013) 2530, [1303.3758].

[2] F. Simon, *Impact of Theory Uncertainties on the Precision of the Top Quark Mass in a Threshold Scan at Future e+e- Colliders*, *PoS* **ICHEP2016** (2017) 872, [1611.03399].

[3] M. Vos et al., *Top physics at high-energy lepton colliders*, 1604.08122.

[4] H. Abramowicz et al., *Top-Quark Physics at the CLIC Electron-Positron Linear Collider*, 1807.02441.

[5] A. Pineda and J. Soto, *Effective field theory for ultrasoft momenta in NRQCD and NRQED*, *Nucl. Phys. Proc. Suppl.* **64** (1998) 428–432, [hep-ph/9707481].

[6] M. Beneke, A. Signer and V. A. Smirnov, *Top quark production near threshold and the top quark mass*, *Phys. Lett.* **B454** (1999) 137–146, [hep-ph/9903260].

[7] N. Brambilla, A. Pineda, J. Soto and A. Vairo, *Potential NRQCD: An Effective theory for heavy quarkonium*, *Nucl. Phys.* **B566** (2000) 275, [hep-ph/9907240].

[8] M. Beneke, A. P. Chapovsky, A. Signer and G. Zanderighi, *Effective theory approach to unstable particle production*, *Phys. Rev. Lett.* **93** (2004) 011602, [hep-ph/0312331].

[9] M. Beneke, A. P. Chapovsky, A. Signer and G. Zanderighi, *Effective theory calculation of resonant high-energy scattering*, *Nucl. Phys.* **B686** (2004) 205–247, [hep-ph/0401002].

[10] M. Beneke, Y. Kiyo, P. Marquard, A. Penin, J. Piclum and M. Steinhauser, *Next-to-Next-to-Next-to-Leading Order QCD Prediction for the Top Antitop S-Wave Pair Production Cross Section Near Threshold in e^+e^- Annihilation*, *Phys. Rev. Lett.* **115** (2015) 192001, [1506.06864].

[11] A. H. Hoang and M. Stahlhofen, *The Top-Antitop Threshold at the ILC: NNLL QCD Uncertainties*, *JHEP* **05** (2014) 121, [1309.6323].

[12] M. Beneke, A. Maier, J. Piclum and T. Rauh, *Higgs effects in top anti-top production near threshold in e^+e^- annihilation*, *Nucl. Phys.* **B899** (2015) 180–193, [1506.06865].

[13] M. Beneke, A. Maier, T. Rauh and P. Ruiz-Femenia, *Non-resonant and electroweak NNLO correction to the e^+e^- top anti-top threshold*, *JHEP* **02** (2018) 125, [1711.10429].

[14] B. Grzadkowski, J. H. Kühn, P. Krawczyk and R. G. Stuart, *Electroweak Corrections on the Toponium Resonance*, *Nucl. Phys.* **B281** (1987) 18–40.

[15] R. J. Guth and J. H. Kühn, *Top quark threshold and radiative corrections*, *Nucl. Phys.* **B368** (1992) 38–56.

[16] A. H. Hoang and C. J. Reisser, *Electroweak absorptive parts in NRQCD matching conditions*, *Phys. Rev.* **D71** (2005) 074022, [hep-ph/0412258].

[17] A. H. Hoang and C. J. Reisser, *On electroweak matching conditions for top pair production at threshold*, *Phys. Rev.* **D74** (2006) 034002, [hep-ph/0604104].

[18] D. Eiras and M. Steinhauser, *Complete Higgs mass dependence of top quark pair threshold production to order alpha alpha(s)*, *Nucl. Phys.* **B757** (2006) 197–210, [hep-ph/0605227].

[19] E. A. Kuraev and V. S. Fadin, *On Radiative Corrections to e+ e- Single Photon Annihilation at High-Energy*, *Sov. J. Nucl. Phys.* **41** (1985) 466–472.

[20] V. S. Fadin and V. A. Khoze, *Threshold Behavior of Heavy Top Production in e+ e- Collisions*, *JETP Lett.* **46** (1987) 525–529.

[21] M. Beneke, B. Jantzen and P. Ruiz-Femenía, *Electroweak non-resonant NLO corrections to e+ e- -> W+ W- b bbar in the t tbar resonance region*, *Nucl. Phys.* **B840** (2010) 186–213, [1004.2188].

[22] A. H. Hoang, C. J. Reisser and P. Ruiz-Femenía, *Phase Space Matching and Finite Lifetime Effects for Top-Pair Production Close to Threshold*, *Phys. Rev.* **D82** (2010) 014005, [1002.3223].

[23] B. Jantzen and P. Ruiz-Femenía, *Next-to-next-to-leading order nonresonant corrections to threshold top-pair production from e^+e^- collisions: Endpoint-singular terms*, *Phys. Rev.* **D88** (2013) 054011, [1307.4337].

[24] J. Alwall, R. Frederix, S. Frixione, V. Hirschi, F. Maltoni, O. Mattelaer et al., *The automated computation of tree-level and next-to-leading order differential cross sections, and their matching to parton shower simulations*, *JHEP* **07** (2014) 079, [1405.0301].

[25] M. Beneke, *A Quark mass definition adequate for threshold problems*, *Phys. Lett.* **B434** (1998) 115–125, [hep-ph/9804241].

[26] M. Beneke, Y. Kiyo, A. Maier and J. Piclum, *Near-threshold production of heavy quarks with QQbar_threshold*, *Comput. Phys. Commun.* **209** (2016) 96–115, [1605.03010].